JCI insight

RESEARCH ARTICLE

Inhibition of bromodomain extraterminal histone readers alleviates skin fibrosis in experimental models of scleroderma

Sirapa Vichaikul,[1] Mikel Gurrea-Rubio,[1] M. Asif Amin,[1] Phillip L. Campbell,[1] Qi Wu,[1,2] Megan N. Mattichak,[1] William D. Brodie,[1] Pamela J. Palisoc,[1] Mustafa Ali,[1] Sei Muraoka,[1] Jeffrey H. Ruth,[1] Ellen N. Model,[1] Dallas M. Rohraff,[1] Jonatan L. Hervoso,[1] Yang Mao-Draayer,[2] David A. Fox,[1] Dinesh Khanna,[1,3] Amr H. Sawalha,[4,5,6,7] and Pei-Suen Tsou[1,3]

[1]Division of Rheumatology and Clinical Autoimmunity Center of Excellence, Department of Internal Medicine, and [2]Department of Neurology, University of Michigan, Ann Arbor, Michigan, USA. [3]University of Michigan Scleroderma Program, Ann Arbor, Michigan, USA. [4]Division of Rheumatology, Department of Pediatrics, University of Pittsburgh School of Medicine, UPMC Children's Hospital of Pittsburgh, Pittsburgh, Pennsylvania, USA. [5]Division of Rheumatology and Clinical Immunology; Department of Medicine; [6]Lupus Center of Excellence; and [7]Department of Immunology, University of Pittsburgh School of Medicine, Pittsburgh, Pennsylvania, USA.

Binding of the bromodomain and extraterminal domain proteins (BETs) to acetylated histone residues is critical for gene transcription. We sought to determine the antifibrotic efficacy and potential mechanisms of BET inhibition in systemic sclerosis (SSc). Blockade of BETs was done using a pan-BET inhibitor, JQ1; BRD2 inhibitor, BIC1; or BRD4 inhibitors AZD5153 or ARV825. BET inhibition, specifically BRD4 blockade, showed antifibrotic effects in an animal model of SSc and in patient-derived diffuse cutaneous SSc (dcSSc) fibroblasts. Transcriptome analysis of JQ1-treated dcSSc fibroblasts revealed differentially expressed genes related to extracellular matrix, cell cycle, and calcium (Ca^{2+}) signaling. The antifibrotic effect of BRD4 inhibition was mediated at least in part by downregulation of Ca^{2+}/calmodulin–dependent protein kinase II α and reduction of intracellular Ca^{2+} concentrations. On the basis of these results, we propose targeting Ca^{2+} pathways or BRD4 as potentially novel therapeutic approaches for progressive tissue fibrosis.

Introduction

Systemic sclerosis (SSc; also called scleroderma) is an autoimmune disease characterized by vascular dysfunction as well as excessive synthesis and deposition of extracellular matrix (ECM) in affected organs. Activation of the immune system and vasculopathy precede fibrosis, in which fibroblast activation and subsequent myofibroblast transdifferentiation are necessary events. At present, SSc is not curable; current treatments focus on managing disease manifestations in an effort to ease the progression of tissue fibrosis.

Although the exact etiology of the disease is not known, a growing body of literature has been pointing to the critical involvement of epigenetic mechanisms in SSc pathogenesis (1). Epigenetic regulation affects chromatin dynamics and thereby modulates gene transcription. In addition to DNA methylation and noncoding RNAs, histone changes are implicated in SSc fibroblast activation (2–4). Acetylation of histones on lysine residues is one of the most common histone modifications that relaxes the chromatin structure by loosening the histone–DNA interaction, which results in increased chromatin accessibility for transcription. Dysregulation of histone acetylation could result in aberrant gene expression, leading to pathogenic consequences. These histone marks, therefore, are tightly regulated by a set of histone acetyltransferases and histone deacetylases. They are also controlled by proteins containing the bromodomain module, such as the bromodomain extraterminal domain (BET) family proteins. The 4 members of the BETs — BRD2, BRD3, BRD4, and the testis-specific BRD-t — share a common domain consisting of 2 N-terminal bromodomains, BD1 and BD2, that bind to acetylated lysine residues on histones. These histone readers provide scaffolds to attract components of the transcriptional machinery to histone acetylation marks. Pharmacological inhibition of BET proteins results in repression of downstream gene expression, thereby modulating various physiological conditions. Indeed, prototype BET inhibitors such as JQ1 or I-BET attenuate various types of cancer and tissue fibrosis (5–9).

Conflict of interest: The authors have declared that no conflict of interest exists.

Submitted: April 26, 2021
Accepted: March 24, 2022
Published: May 9, 2022

Reference information: *JCI Insight*. 2022;7(9):e150871. https://doi.org/10.1172/jci.insight.150871.

Considering the potential antifibrotic properties of BET inhibition, we investigated whether the BET inhibitor JQ1 can modulate fibrogenesis in an animal model of SSc, as well as in dermal fibroblasts isolated from patients with diffuse cutaneous SSc (dcSSc). We posit that BET inhibition impedes the expression of profibrotic genes and blocks myofibroblast differentiation in SSc, thereby improving fibrosis. Through whole transcriptomic analysis, we revealed a mechanism by which BET inhibition exerts its antifibrotic effect in SSc. Furthermore, we demonstrated the involvement of BRD4 in mediating the profibrotic effect of BETs and identified BRD4 as a therapeutic target for this disease. We believe the novelty of our study is that we performed a comprehensive analysis by using both functional assays and transcriptomic analysis, which allowed us to pinpoint a mechanism whereby BET inhibition affects intracellular calcium (Ca^{2+}) and related signaling in SSc fibroblasts. We also show the antifibrotic properties of 2 BRD4 inhibitors, 1 of which, AZD5153, is being evaluated in a clinical trial (ClinicalTrials.gov NCT03205176). To our knowledge, the effect of these inhibitors has not been examined in other fibrotic models before.

Results

The antifibrotic effects of JQ1 in bleomycin-treated mice. To investigate the antifibrotic effect of BET inhibition, we used a pan-BET inhibitor, JQ1, in an animal model of fibrosis. We observed an approximately 3.5% weight reduction in the bleomycin/vehicle group and a 11.4% weight reduction in the bleomycin/JQ1 group. All animals were active without apparent distress throughout the course of the experiment. Daily injections of bleomycin in a defined area in the back of mice increased dermal thickness and collagen accumulation (Figure 1A). Daily JQ1 oral gavage prevented skin fibrosis in bleomycin-treated mice; importantly, attenuation of dermal thickness and collagen was observed. In addition, immunofluorescent staining revealed increased α-SMA– and F4/80-positive cells in bleomycin-treated mice, with F4/80 staining reaching statistical significance (Figure 1B). JQ1 treatment reduced α-SMA– and F4/80-positive cells, with α-SMA staining reaching statistical significance. These results were also reflected at the mRNA level, as profibrotic genes, including *Acta2* and *Col1a1*, whose expression was significantly elevated in bleomycin-treated mice, were downregulated in the presence of JQ1 (Figure 1C). Bleomycin also induced a significant increase in *Il6* and *Ccl2* expression, and both were significantly downregulated with JQ1 treatment. In contrast, *Ctgf* and *Cxcl10* expression were not significantly altered by bleomycin or JQ1.

Antifibrotic properties of BET inhibition in dermal fibroblasts. To further evaluate the effect of BET proteins in SSc fibrosis, we treated dcSSc fibroblasts with JQ1 at various doses (Supplemental Figure 1; supplemental material available online with this article; https://doi.org/10.1172/jci.insight.150871DS1). Given that the highest dose (22 μM) had minimal effect on *CTGF* but upregulated *TGFB1*, suggesting a potential off-target effect, we found that 1 μM appears to be the optimal dose to use. We evaluated the expression of profibrotic genes *COL1A1*, *ACTA2*, *CTGF*, and *TGFB1*, as well as the collagen-degrading enzyme *MMP1* and its inhibitor *TIMP3*. Inhibition of BET by JQ1 led to a dose-dependent decrease in fibrotic markers, including *COL1A1*, *ACTA2*, and *CTGF* (Supplemental Figure 1 and Figure 2A). In addition, JQ1 also increased *MMP1* expression, which is critical for collagen turnover, while it had minimal effect on *TIMP3*. Interestingly, JQ1 significantly increased *TGFB1* expression. This might be an off-target effect of the inhibitor at high doses.

To further characterize the antifibrotic effect of BET inhibition in dcSSc fibroblasts, we performed several functional assays. Treatment with JQ1 dose-dependently reduced migration and proliferation of dcSSc fibroblasts (Figure 2, B and C). The mechanism of reduction of cell proliferation by JQ1 might be due in part to its effect on inducing apoptosis, as JQ1 dose dependently increased apoptotic cells, as indicated by green fluorescence released by activated caspase-3/7, measured using Incucyte live-cell imaging system (Supplemental Figure 2A). However, this effect appears to be delayed, because apoptotic cells appeared after 40 hours, whereas differences in cell proliferation became evident after 30 hours of JQ1 treatment (Figure 2C, right panel, and Supplemental Figure 2A). This finding suggests that other mechanisms are involved in the effect of JQ1 on cell growth. To further analyze the effect of JQ1 on cell growth, we used Vybrant DyeCycle Violet stain to analyze cell cycle distribution in dcSSc fibroblasts. JQ1 induced a reduction in cells in the S phase and accumulation of cells in the G1/G0 phase (Supplemental Figure 2B). Treatment of dcSSc fibroblasts with JQ1 also resulted in a decrease in gel contraction (Figure 2D), with 0.5 μM being the most effective concentration.

Because TGF-β is critical in promoting fibrosis in SSc, we treated normal dermal fibroblasts with TGF-β to induce a myofibroblast phenotype. The induction was confirmed by an increase in cell migration

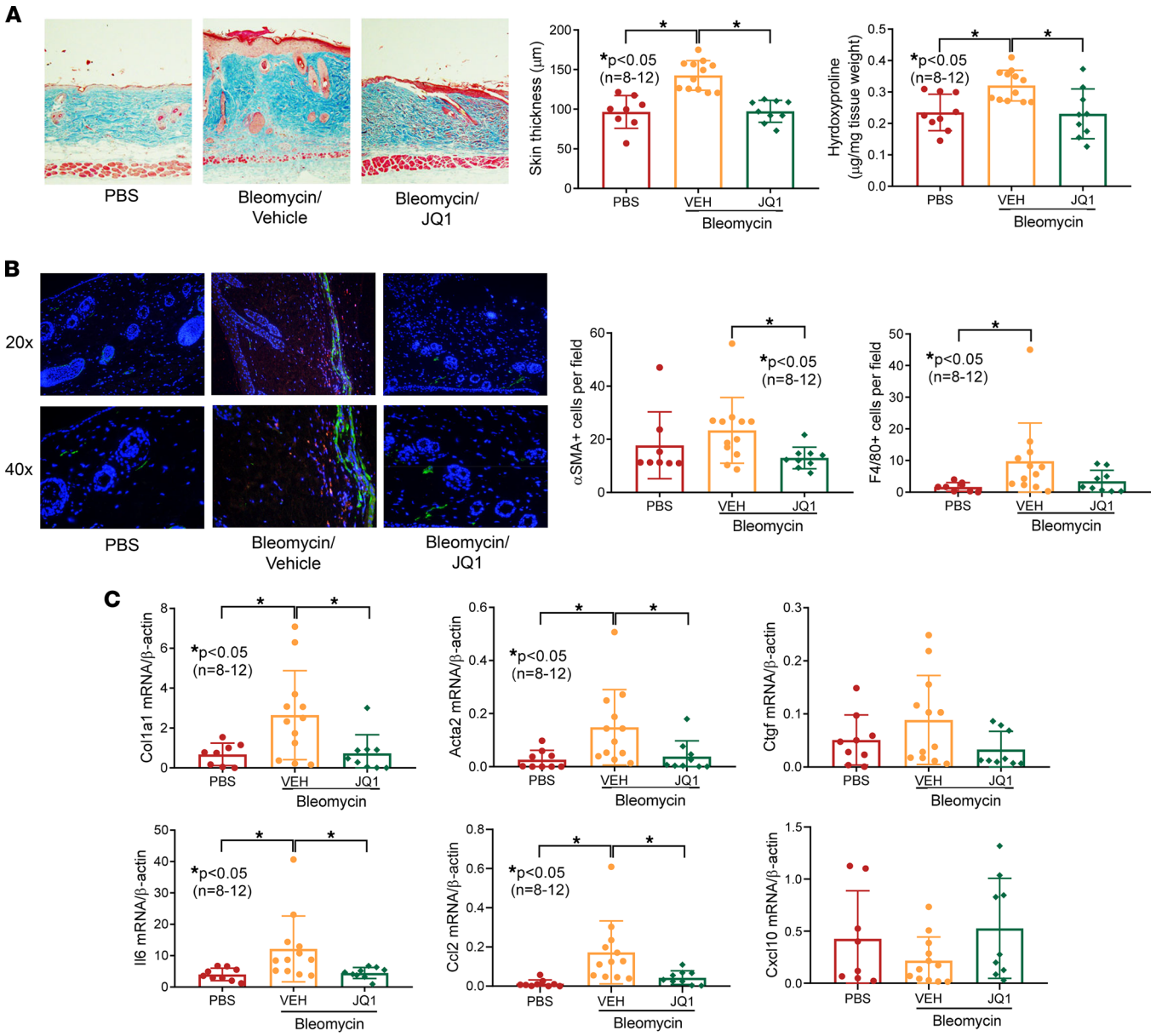

Figure 1. BET inhibition by JQ1 prevents bleomycin-induced skin fibrosis in mice. (**A**) Bleomycin-treated mice showed increased dermal thickness and hydroxyproline content in skin, and JQ1 (50 mg/kg) efficiently prevented skin fibrosis in these mice. Original magnification, ×100. (**B**) Immunofluorescence staining of skin sections showed that JQ1 significantly decreased α-SMA–positive cells (green) in bleomycin-treated mice compared with the vehicle (VEH) group. Similar results were found quantifying F4/80-positive cells (red). Nuclei were stained with DAPI (blue). Original magnification, ×200–400. (**C**) *Acta2*, *Col1a1*, *Il6*, and *Ccl2* were significantly elevated in bleomycin-treated mice and significantly reduced when JQ1 was given. (PBS, $n = 8$; VEH, $n = 12$; JQ1, $n = 9$). Results are expressed as mean ± SD and $P < 0.05$ was considered significant. Significance was determined by 1-way ANOVA (**A** and **C**) and Kruskal-Wallis test (**B** and **C**).

and proliferation, as well as gel contraction in these TGF-β–treated normal fibroblasts compared with non-treated controls (Figure 2, E–G). Cotreatment with JQ1 significantly reduced TGF-β–induced migration, proliferation, and gel contraction in normal dermal fibroblasts.

Transcriptome analysis. To further explore the mechanisms involved in BET inhibition in SSc fibrosis, mRNA-Seq was performed on dcSSc fibroblasts in the absence or presence of 1 μM JQ1. By this analysis, we identified 2113 upregulated and 3499 downregulated genes affected by JQ1 (Figure 3A and Supplemental Figure 3). The excess number of downregulated genes with BET inhibition indicates that BET proteins primarily act as transcription activators in SSc fibroblasts, echoing the findings in other tissues indicating that histone readers are, indeed, transcription activators. The top 20 upregulated and downregulated genes

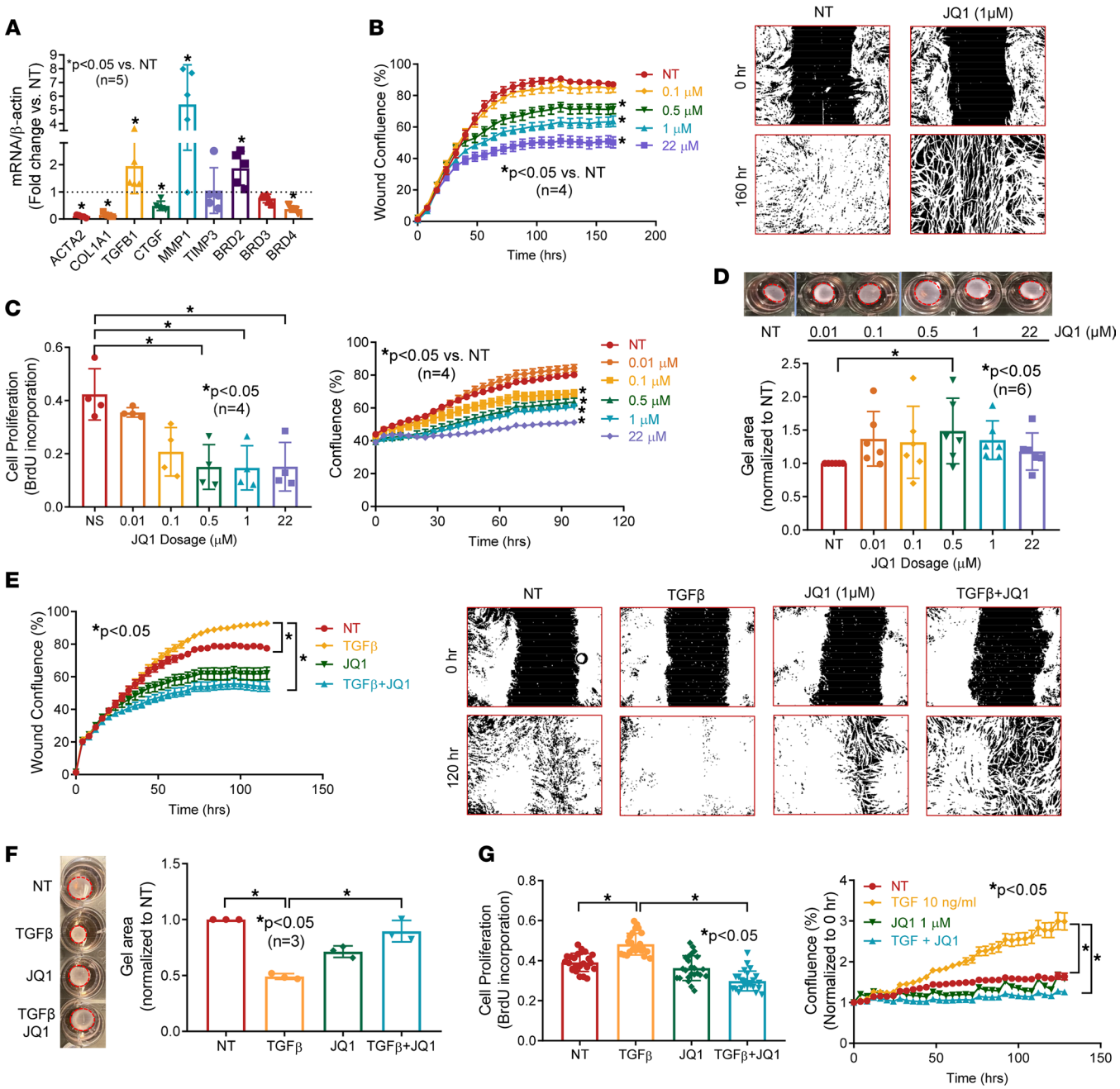

Figure 2. Inhibition of BETs shows potent antifibrotic properties in dcSSc fibroblasts. (**A**) At 1 μM, JQ1 significantly downregulated *ACTA2*, *COL1A1*, *CTGF*, and *BRD4* expression in dcSSc fibroblasts and upregulated *MMP1*, *TGFB1*, and *BRD2*. JQ1 did not affect *TIMP1* and *BRD3* expression. $n = 5$ patients. (**B**) Migration of dcSSc fibroblasts was significantly inhibited by JQ1. Wound confluence indicates the area occupied by cells that migrated into the wound gap. Representative pictures of JQ1 at 1 μM are shown. $n = 4$ patients. (**C**) Inhibition of BETs by JQ1 significantly reduced cell proliferation of dcSSc fibroblasts. Cell growth was analyzed by BrdU uptake in cells or monitored by Incucyte live-cell imaging system. $n = 4$ patients. (**D**) Gel contraction by dcSSc fibroblasts was inhibited by JQ1 at 0.5 μM. $n = 6$ patients. (**E**–**G**) Cell migration ($n = 4$), proliferation ($n = 4$), and gel contraction ($n = 3$) significantly increased after TGF-β treatment in normal dermal fibroblasts and can be inhibited by coincubation of 1 μM JQ1. Results are expressed as mean ± SD or mean ± SEM (time courses in **B**, **C**, **E**, and **F**); $P < 0.05$ was considered significant. Significance was determined by unpaired 2-tailed *t* test and Mann-Whitney *U* test (**A**), 2-way ANOVA (**B**, **C**, **E**, and **G**), 1-way ANOVA (**F**), and Kruskal-Wallis test (**D** and **G**). NT, no treatment.

are shown in Figure 3B. In addition, RNA-Seq results confirmed expression changes observed using quantitative PCR in fibrosis-related genes (Figure 2A): *ACTA2* and *COL1A1* were significantly downregulated while *TGFB1* and *BRD2* were significantly upregulated at 1 μM JQ1 treatment (Supplemental Figure 4).

Further pathway enrichment analysis of the differentially expressed genes regulated by JQ1 revealed that these genes are enriched in Kyoto Encyclopedia of Genes and Genomes (KEGG) pathways, including

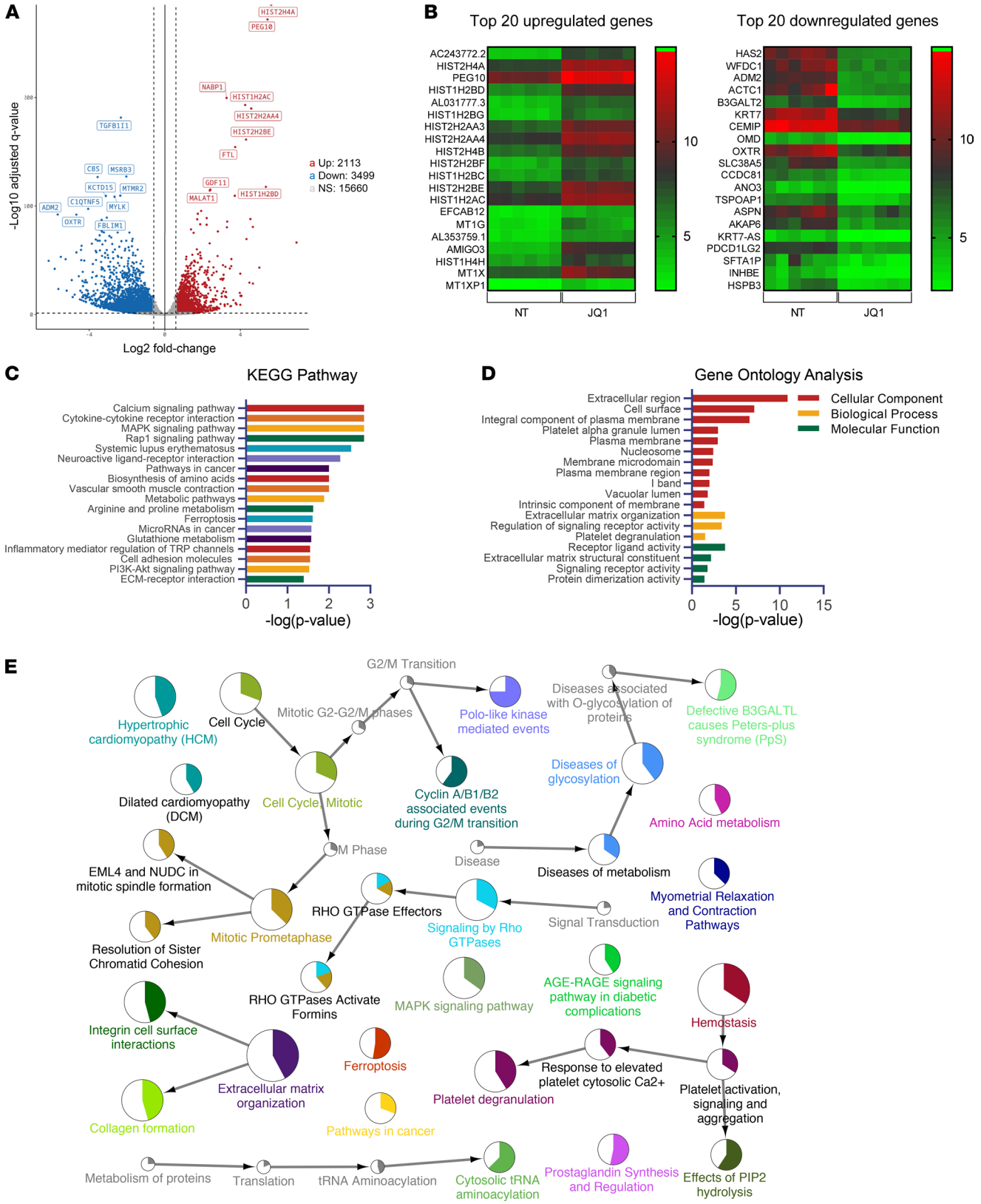

Figure 3. JQ1 treatment followed by RNA-Seq identified targets important for ECM remodeling, cell cycle regulation, and signaling in dcSSc fibroblasts. (**A**) A total of 6 patient pairs were used for RNA-Seq analysis. In total, 5612 genes were significantly differentially expressed by JQ1 treatment in dcSSc fibroblasts (3499 downregulated and 2113 upregulated). (**B**) Top 20 upregulated and downregulated genes were shown. (**C**) The 18 most significantly enriched KEGG pathways after treatment with JQ1 in dcSSc fibroblasts are shown. (**D**) Gene Ontology analysis of the differentially expressed genes after JQ1 treatment in dcSSc fibroblasts. (**E**) Network of functional categories represented by JQ1-associated changes in dcSSc fibroblasts based

on functional enrichment analysis. The node size corresponds with the level of significance (*P* value range, <0.05 to <0.0005) of the term it represents within the network. Colored portions of the pie charts represent the number of genes identified from the RNA-Seq experiment that are associated with the term. NT, no treatment. TRP, transient receptor potential.

the Ca^{2+} signaling pathway, cytokine–cytokine receptor pathway, MAPK and Rap1 signaling pathways, as well as metabolic pathways, among others (Figure 3C and Supplemental Table 1). In addition, Gene Ontology analysis showed that BET proteins are involved in a wide spectrum of cellular components, biological processes, and molecular functions known to play critical roles in fibroblast activation (Figure 3D). These include ECM, plasma membrane, and signaling-receptor activity.

To better visualize the network of functional categories represented by JQ1-associated changes, we performed additional functional enrichment analysis using ClueGO/CluePedia by incorporating the KEGG, Reactome, and WikiPathways. As shown in Figure 3E, networks related to cell cycle regulation, ECM organization, signaling by Rho GTPases, ferroptosis, homeostasis, and diseases of glycosylation, among others, were significantly enriched.

We also examined the subcellular localization of the enriched pathways using the cerebral layout tool implemented in Cytoscape. The subcellular localization of JQ1-affected pathways was skewed toward ECM and plasma membranes (Supplemental Figure 5). This is not surprising, as functions related to ECM and homeostasis, as well as signaling pathways, were among the most enriched (as demonstrated by the size of the nodes). Indeed, when the differentially expressed genes were overlaid on the ECM–receptor interaction pathway (KEGG pathway 04512), many ECM genes and their binding partners were affected by JQ1, with the majority of these genes being downregulated (Supplemental Figure 6). In the intracellular compartment and the nucleus, cell cycle regulation is the main enriched pathway (Supplemental Figure 5). These results echo our functional data shown in Figure 2 and Supplemental Figure 2, as JQ1 showed strong antiproliferative and antifibrotic effects in these cells. Finally, as expected, the predicted upstream regulator analysis showed JQ1 as the most significant upstream chemical: 1521 genes from our transcriptomic analysis overlapped with reported JQ1-target genes (Supplemental Figure 7). This finding not only validates the JQ1 inhibition condition and sequencing analysis used in this study but also shows that genes affected by BET inhibition are common among different biological systems and cell types.

BET inhibition affects the Ca^{2+} signaling pathways in dcSSc fibroblasts. As shown in Figure 3C, the most significant enrichment of the differentially expressed genes in the KEGG pathways was in the Ca^{2+} signaling pathway. To better visualize the location of the differentially expressed genes, we overlaid them in the pathway. JQ1 appeared to affect genes involved in Ca^{2+} channels on the plasma membrane, Ca^{2+} receptors that are located in the ER or sarcoplasmic reticulum, Ca^{2+}-related signaling pathways, and Ca^{2+}-dependent downstream effectors (Figure 4A). All the differentially expressed genes enriched in this pathway are listed in Figure 4B. Of the 59 genes, 15 were upregulated by JQ1, again pointing to BET proteins as transcriptional activators.

Because Ca^{2+} signaling affects fibroblast function and myofibroblast transformation (10), we examined whether JQ1 affects intracellular Ca^{2+} levels in dcSSc fibroblasts. As shown in Figure 4C, JQ1 significantly reduced intracellular Ca^{2+} levels in dcSSc fibroblasts.

JQ1 mediates its antifibrotic effect in part by affecting Ca^{2+} signaling in dcSSc fibroblasts. To further examine the involvement of intracellular Ca^{2+} in the antifibrotic effect of JQ1, we cultured dcSSc fibroblasts in the presence or absence of Ca^{2+} and treated the cells with or without JQ1. Comparing the nontreated groups in the presence or absence of Ca^{2+} in culture medium, the expression of *ACTA2* and *COL1A1* was significantly lower in cells cultured in medium without Ca^{2+} (Figure 5A). JQ1 significantly downregulated *ACTA2* and *COL1A1* in Ca^{2+}-containing media, and JQ1's effect on *COL1A1* was diminished in medium without Ca^{2+}. Using BAPTA-AM, an intracellular Ca^{2+}-chelating reagent, we also showed that depleting Ca^{2+} in cells decreased *ACTA2* and *COL1A1* expression, and the inhibitory effect of JQ1 on these genes was blocked (Figure 5B). To further demonstrate the involvement of Ca^{2+} in the antifibrotic effect of JQ1, we focused on *CAMK2A*, which encodes Ca^{2+}/calmodulin–dependent protein kinase II α (CaMKII-α), in subsequent studies. This gene is central for Ca^{2+}-mediated effects in cells and was significantly downregulated by JQ1 (Figure 4, A and B). We further confirmed the effect of JQ1 on *CAMK2A* expression by quantitative PCR (Figure 5C). Overexpression of *CAMK2A* in dcSSc fibroblasts blocked the inhibitory effect of JQ1 on *COL1A1* expression (Figure 5C) but not on *ACTA2*. Because members of the CaMKII family are involved in regulating the cell cycle (11), we examined whether *CAMK2A* is involved in JQ1-mediated

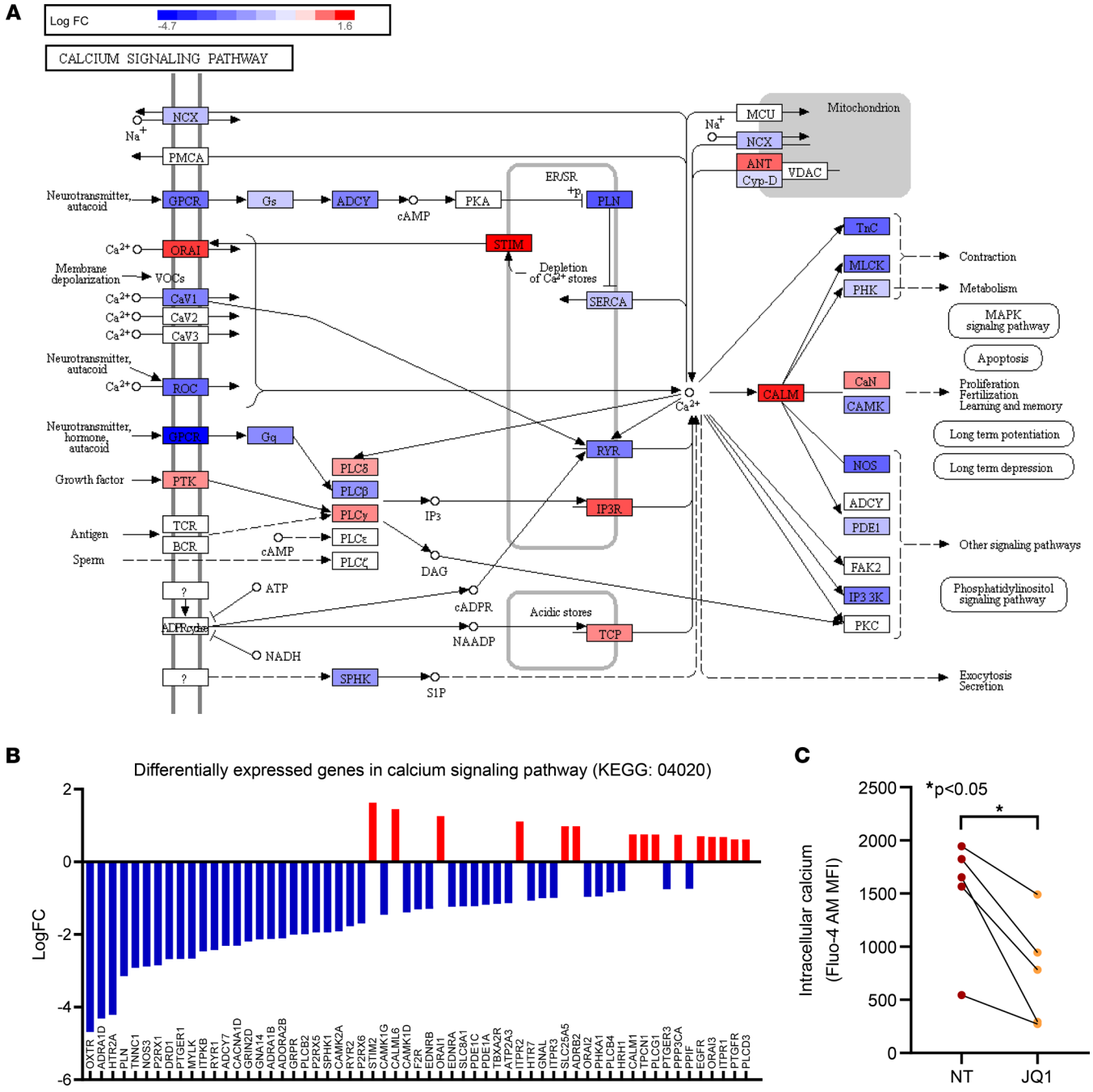

Figure 4. BET inhibition affects Ca^{2+}-related pathways and intracellular Ca^{2+} in dcSSc fibroblasts. (**A**) The Ca^{2+} signaling pathway (KEGG: 04020) diagram is overlaid with the expression changes of each gene. The legend describes the values on the gradient. Downregulation is shown in blue, while upregulation is in red. For legibility, 1 gene may be presented at multiple boxes in the diagram. In addition, 1 box may represent multiple genes in the same gene family. For each gene family, the color corresponding to the gene with the highest absolute fold change is displayed. For example, the ORAI box depicts significant upregulation of *ORAI1* and *ORAI3* and downregulation of *ORAI2*. The ORAI box is shown in red because *ORAI1* shows the most significant fold change among the 3. (**B**) All the differentially expressed genes in Ca^{2+} signaling pathway (KEGG: 04020) are ranked based on their absolute value of log fold change. Upregulated genes are shown in red, and downregulated genes are shown in blue. n = 6 patient pairs. (**C**) BET inhibition by JQ1 significantly reduced intracellular Ca^{2+} levels in dcSSc fibroblasts. n = 5 patients. Results are expressed as mean ± SD and $P < 0.05$ was considered significant. Significance was determined by paired 2-tailed t test (**C**). NT, no treatment.

antiproliferative effect in dcSSc fibroblasts. Indeed, we found that *CAMK2A* appears to be involved, at least in part, in the antiproliferative effect of JQ1, because overexpression of *CAMK2A* resulted in an approximately 25% reduction in cell growth by JQ1 compared with 50% in the control group (Figure 5D). Notably, *CAMK2A* overexpression in dcSSc fibroblasts not only resulted in elevated levels of *ACTA2* and

COL1A1 but also increased cell proliferation, suggesting that this gene plays a critical and nonredundant role in promoting SSc fibrosis. These results support the involvement of Ca^{2+} and Ca^{2+}-related pathways in the antifibrotic effect of JQ1, specifically on collagen expression and cell proliferation.

BET expression in SSc. We examined the expression of BET proteins in dermal fibroblasts. Of the 4 BETs, BRD-t is expressed predominantly in the testis and therefore was excluded from our study. At the mRNA level, only *BRD4* was significantly upregulated in dcSSc fibroblasts, compared with normal fibroblasts (Supplemental Figure 8A). At the protein level, however, the expression of the BETs was variable in dcSSc fibroblasts, but no difference between normal and dcSSc was seen (Supplemental Figure 8B).

BRD4 is profibrotic. Because JQ1 is a pan-BET inhibitor, we next performed a set of experiments to determine which BET is responsible for the antifibrotic effect of JQ1. JQ1 significantly induced *BRD2* and decreased *BRD4*, whereas it had minimal effect on *BRD3* (Supplemental Figure 1 and Figure 2A). We then knocked down BRD2, BRD3, or BRD4 individually and examined the expression of genes involved in fibrosis. As shown in Figure 6A, knockdown of BRD2 resulted in significant elevation of *COL1A1* expression, whereas knockdown of BRD4 led to significant reduction of *COL1A1*, *ACTA2*, *TGFB1*, *CTGF*, and *MMP1* expression. BRD3 knockdown decreased *TIMP3* expression and had no effect on the other genes examined. In addition, BRD4 knockdown led to significant reduction in gel contraction (Figure 6B), suggesting that BRD4 is profibrotic and that JQ1, by significantly reducing BRD4 expression in dcSSc fibroblasts, inhibits fibrosis in SSc.

To confirm the involvement of BRD2 and BRD4 in myofibroblast function, we treated dcSSc fibroblasts with a specific BRD2 inhibitor (BIC1) or BRD4 inhibitors (AZD5153 or ARV825). As shown in Figure 7A, inhibition of BRD2 by BIC1 did not affect dcSSc fibroblast proliferation; BRD4 inhibition by either AZD5153 or ARV825 significantly inhibited proliferation at both 1 and 10 μM. In addition, dcSSc fibroblasts treated with BRD4 inhibitors ARV825 or AZD5153 significantly reduced *ACTA2* and *COL1A1* expression, whereas BRD2 inhibitor BIC1 did not have any effect (Figure 7B). Similar results were observed at the protein level (Figure 7C).

To further determine the antifibrotic effect of BRD4 inhibition in vivo, we induced skin fibrosis by bleomycin in mice and dosed the animals with either ARV825 or AZD5153. We found that both BRD4 inhibitors prevented bleomycin-induced skin fibrosis in mice, as indicated by dermal thickness, α-SMA–positive cells, and hydroxyproline content (Figure 7D). These results further confirm the involvement of BRD4 in myofibroblast transformation in dcSSc fibroblasts and in the bleomycin mouse model.

BRD4 mediates its fibrotic properties through Ca^{2+} signaling in dcSSc fibroblasts. To further investigate whether BRD4 inhibitors affect intracellular Ca^{2+} in dcSSc fibroblasts similar to what was observed with JQ1, we measured intracellular Ca^{2+} levels in the presence or absence of the BRD4 inhibitors. We found that both inhibitors decreased intracellular Ca^{2+} levels after 48 hours of treatment, with AZD5153 reaching statistical significance (Figure 7E). Interestingly, the BRD2 inhibitor BIC1 significantly increased intracellular Ca^{2+} levels, suggesting that this BET isoform could act in an opposite way than BRD4 in dcSSc fibroblasts. We further showed that both BRD4 inhibitors downregulated *CAMK2A* in dcSSc fibroblasts (Figure 7F). In addition, the antifibrotic effects of both AZD5153 and ARV825 in dcSSc fibroblasts were partially dependent on *CAMK2A*. Overexpression of *CAMK2A* in these cells appeared to block the inhibitory effect of AZD5153 on *COL1A1* (Figure 7F), whereas it had minimal effect on *ACTA2* expression. BRD4 inhibitors also blocked cell proliferation by 50% in control cells but only by approximately 25% in the *CAMK2A*-overexpressing cells, suggesting that *CAMK2A* is partially involved in BRD4-mediated effects on cell growth (Figure 7G).

Discussion

The increased understanding of the effect of epigenetic aberrations on gene transcription has led the field to a better appreciation of the role of transcriptional dysregulation in initiating and perhaps maintaining SSc fibrosis. In this study, we performed an in-depth examination of BET inhibition in SSc fibrosis. Our in vivo studies showed that administration of JQ1 prevented skin fibrosis induced by bleomycin in mice. We further demonstrated that BET inhibition by JQ1 suppressed expression of many profibrotic genes in dcSSc fibroblasts and reversed the established progression of myofibroblast differentiation in vitro. Transcriptomic analysis of JQ1-treated cells not only showed that differentially expressed genes are enriched in ECM- and cell cycle–related pathways but also revealed the involvement of the Ca^{2+} signaling pathway as a novel antifibrotic mechanism. Moreover, results from siRNA knockdown experiments confirmed the role of BRD4 in SSc fibrosis. This was further confirmed using

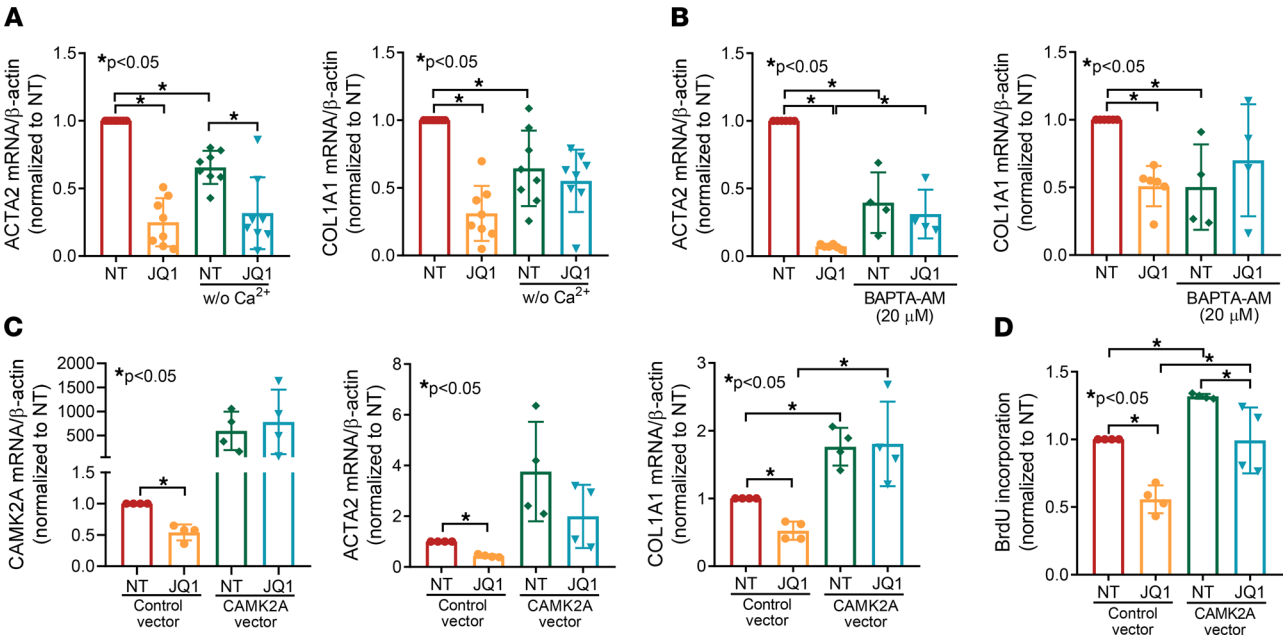

Figure 5. The antifibrotic effect of JQ1 is abolished by the sequestration of intracellular Ca^{2+} and overexpression of *CAMK2A* in dcSSc fibroblasts. (**A**) Cells cultured in Ca^{2+}-free media had lower levels of *ACTA2* and *COL1A1* compared with cells cultured in Ca^{2+}-containing media. The effect of JQ1 on COL1A1 is blocked in cells cultured without Ca^{2+}. n = 8 patients. (**B**) BAPTA-AM, an intracellular Ca^{2+}-chelating reagent, significantly decreased *ACTA2* and *COL1A1* expression in dcSSc fibroblasts. It also blocked the effect of JQ1. n = 4 patients. (**C**) JQ1 downregulated *CAMK2A* expression in dcSSc fibroblasts. Overexpression of *CAMK2A* not only increased *ACTA2* and *COL1A1* expression, but it also blocked the antifibrotic effects of JQ1. n = 4 patients. (**D**) *CAMK2A* is critical for cell proliferation, as overexpression of this gene enhanced cell proliferation. The inhibitory effect of JQ1 on cell proliferation was blocked by *CAMK2A* overexpression. n = 4 patients. Results are expressed as mean ± SD and $P < 0.05$ was considered significant. Significance was determined by 1-way ANOVA. NT, no treatment.

BRD4-specific inhibitors. Functional studies showed that Ca^{2+} and the Ca^{2+}-related gene *CAMK2A* play critical roles in the antifibrotic effects of JQ1, AZD5153, and ARV825. Together, these results suggest that BRD4 is critically involved in promoting fibrosis in SSc, and that inhibition of BRD4, and perhaps targeting intracellular Ca^{2+}, would be effective treatments for this disease.

JQ1, a first-in-class BET inhibitor, competitively binds to the acetyl-lysine recognition areas of these proteins and displaces them from acetylated chromatin, thereby repressing transcription of target genes. Early studies suggested that JQ1 exerted potent antiproliferative properties in multiple myeloma via cell growth arrest and senescence in a c-MYC–dependent manner (12). Since then, more studies have shown the benefits of JQ1 in other proliferative disorders (5–8). In addition, this pan-BET inhibitor has demonstrated great efficacy in blocking fibrotic progression in a range of fibrosis models (5–8). In a lung fibrosis model, JQ1 significantly reduced collagen deposition in bleomycin-treated mice compared with control mice (8). This drug also ameliorated the phenotypic changes of lung fibroblasts from patients with idiopathic pulmonary fibrosis. We showed in this study that JQ1 inhibits proliferation of dcSSc dermal fibroblasts by inducing cell cycle arrest and apoptosis. It also exhibits potent antifibrotic effects in patient-derived cells and in the bleomycin skin-fibrosis model. The functional changes in cell proliferation were also confirmed from the RNA-Seq results, as genes enriched in cell cycle, mitosis, and ferroptosis pathways were highlighted in the pathway analysis (Figure 3E). Our results are consistent with the findings of Shin et al. (13), who showed that JQ1 repressed collagen expression in SSc skin organ culture, likely due to the increase in MMP1.

BET proteins are located in the nucleus. Because of their involvement in various cellular processes, BETs have been shown to participate in tumor development, autoimmunity, infections, and inflammation (14–17). Specifically, BRD4 has been studied extensively for its role in gene transcription, including regulation (through acetylated histones), initiation (via engaging RNA polymerase II), and elongation (by interaction with P-TEFb) (18). Indeed, BRD4 is reported to control various fibrosis-related genes, including *ACTA2* and *COL1A1*, shown from BRD4 knockdown studies or ChIP analyses (5, 7, 8, 19). This is not surprising, because both genes are reported to possess acetylated histones in their promoter region in fibroblasts (Supplemental Figure 9). In dcSSc fibroblasts, inhibition of BETs by JQ1 downregulated both

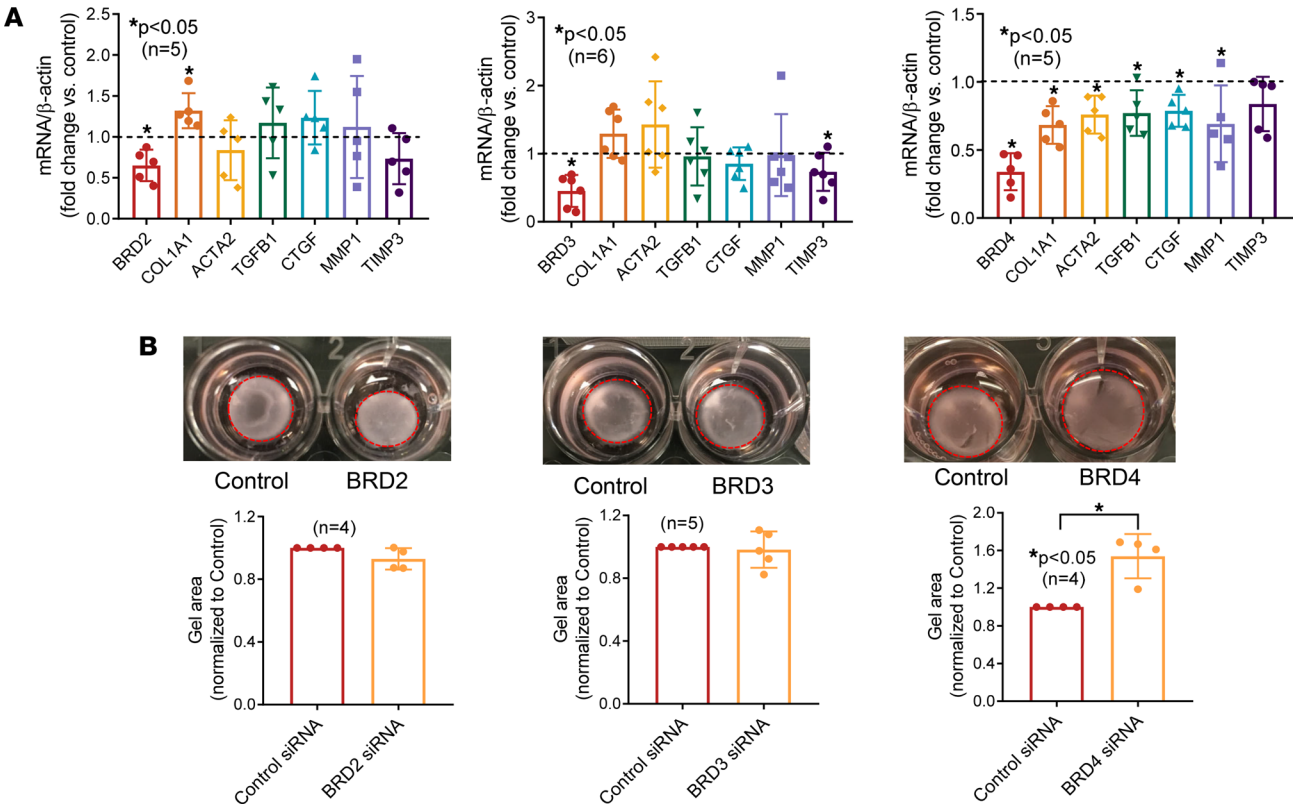

Figure 6. BRD4 mediates the profibrotic effect of BETs in dcSSc fibroblasts. (**A**) BRD2 knockdown in dcSSc fibroblasts led to upregulation of *COL1A1*, and BRD3 knockdown resulted in downregulation of *TIMP3*. Knockdown of BRD4 resulted in downregulation of *COL1A1*, *ACTA2*, *TGFB*, *CTGF*, and *MMP1*. n = 5–6 patients. (**B**) BRD4 knockdown significantly inhibited gel contraction in dcSSc fibroblasts, whereas BRD2 or BRD3 knockdown had minimal effect on gel contraction. n = 4–5 patients. Results are expressed as mean ± SD and $P < 0.05$ was considered significant. (**A** and **B**) Significance was determined by unpaired 2-tailed t test or Mann-Whitney U test.

ACTA2 and *COL1A1*, and this downregulation appears to be mediated through blockade of BRD4, because BRD4 knockdown or inhibition led to decreased *ACTA2* and *COL1A1* levels, while knockdown of BRD2 or BRD3 did not. Interestingly, *TGFB1*, which was significantly upregulated by JQ1, was downregulated in BRD4–knocked-down cells. Similar results were seen in *MMP1* expression. This discrepancy suggests that JQ1, as a pan-BET inhibitor, has off-target effects compared with BRD4 knockdown, especially at the higher concentrations. This could potentially explain the U-shaped dose-response curve of JQ1 in the gel contraction assay. Of note, our results showing that BRD2 knockdown leads to *COL1A1* upregulation are consistent with those in previous reports (19). Because JQ1 dose-dependently increased *BRD2* expression in dcSSc fibroblasts, it is possible that the antifibrotic effect of JQ1 is partly mediated by enhancing the antifibrotic potential of BRD2. However, BRD2 inhibition, although trending to induction of fibroblast migration and profibrotic gene expression (Figure 7, A–C), had no significant effect on enhancing myofibroblast functions. Furthermore, BIC1 significantly increased intracellular Ca^{2+} levels in dcSSc fibroblasts, in contrast to BRD4 inhibition.

To gain mechanistic insight into the antifibrotic effect of BET inhibition in SSc, we performed mRNA-Seq in JQ1-treated dcSSc fibroblasts. In addition to pathways in cell cycle regulation, ECM, and intracellular signaling, our analysis also revealed potentially novel pathways, including Ca^{2+} signaling, metabolism, ferroptosis, and prostaglandin synthesis and regulation (Figure 3E). These pathways have been implicated in various fibrotic conditions; thus, it is possible that they are involved in the antifibrotic effect of BET inhibition in dcSSc fibroblasts. Specifically, the Ca^{2+} signaling pathway, which is the most enriched pathway in our analysis (Figure 3C), is critical in various fibrotic conditions (10, 20, 21). Intracellular Ca^{2+} levels are controlled by Ca^{2+}-permeable channels in the plasma membrane (voltage-operated channels and receptor-operated channels), Ca^{2+} release from the ER and sarcoplasmic reticulum, as well as Ca^{2+} extrusion pumps. The increase in intracellular Ca^{2+} levels can activate various pathways that are involved in many physiological functions

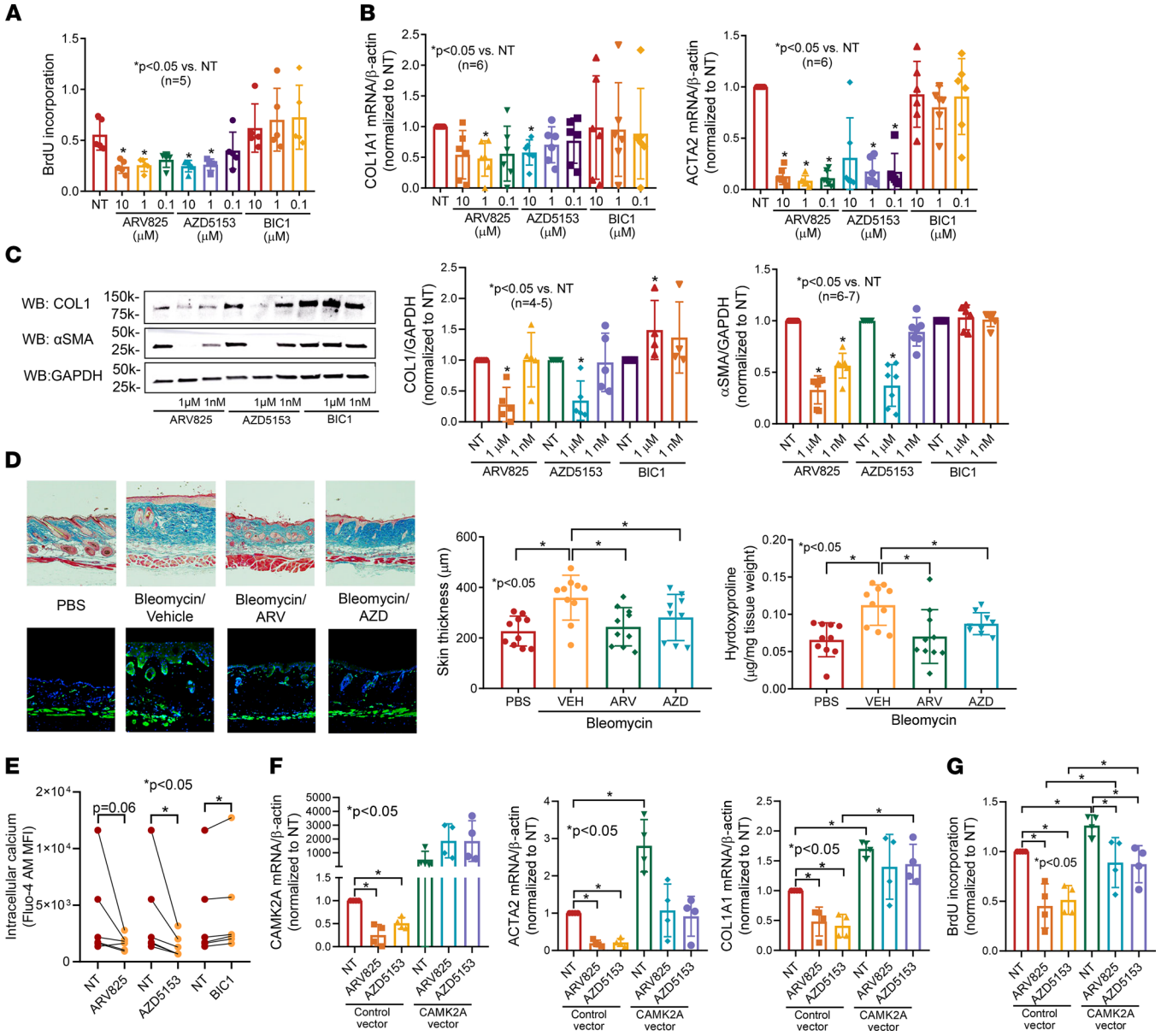

Figure 7. BRD4 inhibitors show prominent antifibrotic effects in vitro and in vivo. (**A**) Treating dcSSc fibroblasts with the specific BRD2 inhibitor BIC1 had minimal effect on cell proliferation, whereas inhibition of BRD4 using BRD4 inhibitors AZD5153 or ARV825 significantly reduced cell proliferation at concentrations of 1 and 10 μM. n = 5 patients. (**B**) Inhibition of BRD4 by ARV825 or AZD5153 in dcSSc fibroblasts significantly reduced both *ACTA2* and *COL1A1* expression, whereas blockade of BRD2 by BIC1 had no effect. n = 6 patients. (**C**) BRD4 inhibitors significantly decreased α-SMA (n = 7) and COL1 (n = 5) in dcSSc fibroblasts, whereas BRD2 inhibition by BIC1 had minimal effect on α-SMA (n = 6) but increased COL1 at 1 μM (n = 4 patients). (**D**) Bleomycin-treated mice had increased dermal thickness and hydroxyproline content in skin, and ARV825 or AZD5153 efficiently prevented skin fibrosis in these mice. Immunofluorescence staining of α-SMA–positive cells (green) is shown. Nuclei were stained with DAPI (blue). Original magnification, ×40–100. n = 9–10 mice. (**E**) BRD4 inhibitor AZD5153 significantly decreased intracellular Ca^{2+} and BRD2 inhibitor BIC1 significantly increased it. n = 6 patients. (**F**) Overexpression of *CAMK2A* resulted in significant increase in *ACTA2* and *COL1A1* expression and blocked the effect of AZD5153 on *COL1A1* expression. n = 4 patients. (**G**) *CAMK2A* overexpression significantly increased cell proliferation while it abolished the effect of BRD4 inhibition on cell proliferation. n = 4 patients. Results are expressed as mean ± SD and $P < 0.05$ was considered significant. Significance was determined by 1-way ANOVA (**A**–**D**, **F**, and **G**), Kruskal-Wallis test (**A**–**C**), and Wilcoxon's test (**E**). NT, no treatment.

(22–25). Studies show that interference of intracellular Ca^{2+} levels through blockade of Ca^{2+} channels or receptors has potential antifibrotic effects in various models (26–29). In dcSSc fibroblasts, JQ1 treatment significantly reduced Ca^{2+} levels in these cells (Figure 4C). This is possibly mediated by significant downregulation of Ca^{2+} channels and receptors on the plasma membrane, including *P2RX1* and *P2RX5* (coding for purinergic receptors P2X1 and P2X5), calcium voltage-gated channel subunit α-1D (*CACNA1D*), and voltage-dependent Ca^{2+} channel protein TPC1 (*TPCN1*), as well as ones on the ER and sarcoplasmic reticulum,

such as ryanodine receptor 1 (*RYR1*) (Figure 4B). Interestingly, certain Ca^{2+} channels, Ca^{2+} extrusion pumps, and Ca^{2+} release transporters that increase intracellular Ca^{2+} were affected by JQ1. It is possible that these events represent a compensatory mechanism that attempts to antagonize the decreased Ca^{2+} levels in these fibroblasts. The identification of Ca^{2+} pumps, carriers, and channels involved in Ca^{2+} entry, as well as their involvement in mediating the fibrotic effect of BET proteins in SSc, requires further investigation.

In this study, we identified CaMKII, specifically the α isoform, as a critical mediator of the fibrotic effect of BETs and BRD4. CaMKII, composed of 4 isoforms, is a downstream messenger of the Ca^{2+} signaling pathway. CaMKII activation augmented collagen production in cardiac fibroblasts, while inhibition of CaMKII blocked proliferation and collagen and profibrotic cytokine production (22, 30, 31). We showed similar findings in dcSSc fibroblasts in this study in the context of the BET or BRD4 inhibitors. In addition to cardiac fibrosis, CaMKII is also involved in pulmonary fibrosis (32), ureteral scar formation (33), and renal fibrosis (34). CaMKII is associated with FGFR3/FGF9 in SSc fibroblasts, functioning as a downstream mediator of the profibrotic effect of FGFR3 (25). Interestingly, our results showed that *CAMK2A* appears to play a more critical role in BET or BRD4-mediated *COL1A1* expression in dcSSc fibroblasts, but not as important a role in blocking myofibroblast transformation. *CAMK2A* only partially explains the proliferative effects of BET or BRD4, as shown in Figures 5 and 7. These results point to the possibility of other mediators being involved in the antifibrotic effects of BET and BRD4 inhibitors. Intriguingly, we found that overexpression of *CAMK2A* alone led to significant increase in fibrotic gene expression and cell proliferation in dcSSc fibroblasts, suggesting that this gene itself could play a critical role in SSc fibrosis.

Although JQ1 possesses desirable qualities of a small molecular inhibitor, including high target potency and well-characterized selectivity, it is known for its inhibitory effect on lymphoid and hematopoietic tissues (35). JQ1 exhibits linear pharmacokinetics in mice, with an oral bioavailability of approximately 50% and a half-life of 1 hour (35, 36). Due to the short half-life and potential off-target effects, this compound is only used in preclinical studies. Currently, there are several BET inhibitors with better pharmacokinetic properties in clinical trials for various types of cancer (9). Recent trials have also focused on targeting specific BETs, including BRD4 inhibitors AZD5153 (ClinicalTrials.gov NCT03205176), which was used in this study, and ABBC-744 (ClinicalTrials.gov NCT03360006). Based on our results, BETs, in particular BRD4, regulate essential processes involved in SSc fibrosis. We not only revealed an antifibrotic mechanism involving Ca^{2+} signaling by BET inhibition but also highlighted the potential of epigenetic therapeutic strategies targeting BRD4 for patients with SSc. These data, along with future studies focusing on additional molecular mechanisms underlying the role of BRD4 in SSc, should provide the framework that supports the use of more selective BRD4 inhibitors as a therapeutic option for SSc.

Methods

Bleomycin-induced skin fibrosis. The procedure to induce fibrosis by bleomycin in mice was published previously (2, 37). In C57BL/6 mice (The Jackson Laboratory, 000664), 100 μL of bleomycin (1 mg/mL) or PBS was injected s.c. into a single location on the shaved back once every day for 2 weeks. JQ1 (50 mg/kg; MedChemExpress) or vehicle control (20% DMSO, 50% PBS, 30% PEG from J.T.Baker) was given daily by oral gavage. In a separate experiment, BRD4 inhibitors AZD5153 (5 mg/kg; Cayman Chemical) or ARV825 (5 mg/kg, MedChemExpress) or vehicle control (22% DMSO, 48% PBS, 30% PEG) were given daily i.p. At the end of the experiment, fixed skin sections were stained with Masson's trichrome. Dermal thickness was measured by analyzing the distance between the epidermal–dermal junction and the dermal–fat junction in 3 fields in 2 or more skin sections from each animal. Immunofluorescence was performed on sections using anti–α-SMA (Abcam ab5694) or anti-F4/80 (Invitrogen MA5-16630; clone CI:A3-1) Abs after antigen-retrieval. Collagen content in the skin was measured using the Hydroxyproline Kit (Abcam). All animal protocols were approved by the IACUC at the University of Michigan.

Patients and control participants. All patients recruited from the University of Michigan Scleroderma Program in this study met the American College of Rheumatology and European Alliance of Associations for Rheumatology criteria for the classification of SSc (38). Punch-biopsy specimens from the distal forearm of healthy volunteers and patients with dcSSc were obtained for fibroblast isolation. This study was approved by the University of Michigan IRB. The demographics and clinical characteristics of the enrolled individuals are summarized in Supplemental Table 2.

Cell culture. Punch-biopsy specimens obtained from healthy study participants and patients with SSc were digested as previously described (2, 39). Briefly, biopsy specimens were placed in 2.4 U/mL dispase (Invitrogen)

overnight at 4°C. After removing the epidermal layers, the biopsy specimens were transferred to a 0.2% collagenase solution (MilliporeSigma) and incubated at 37°C for 45 minutes. The dissociated cells were then collected and cultured. After separating out the endothelial cells by magnetic bead selection (CD31 MicroBead Kit from Miltenyi Biotec), the resultant fibroblasts were maintained in RPMI-1640 medium (Hyclone) supplemented with 10% FBS and antibiotics. Cells between passage 3 and 6 were used in all experiments.

Cell treatment and transfection. Dermal fibroblasts from patients with dcSSc were treated with 0.01 to 22 μM JQ1 (Cayman Chemical), a pan-BET inhibitor, for 48 hours. Normal dermal fibroblasts were treated with TGF-β (10 ng/mL; Cell Signaling Technology) and/or JQ1 (1 μM) for 72 hours to induce a myofibroblast phenotype. In a separate experiment, BRD2 inhibitor BIC1 (Cayman Chemical) and BRD4 inhibitors AZD5153 or ARV825 (0.1–10 μM; Cayman Chemical) were used to treat dcSSc fibroblasts for 48 to 72 hours. BRD2, BRD3, or BRD4 knockdown in dcSSc dermal fibroblasts was performed using *BRD2* (200 nM), *BRD3* (100 nM), or *BRD4* (200 nM) siRNA (ON-TARGETplus siRNA; Dharmacon). Scrambled siRNA (Dharmacon) was used as a control. The cells were transfected for 72 hours before downstream experiments were performed. *CAMK2A* in dcSSc fibroblasts was overexpressed using *CAMK2A* vectors from OriGene. *CAMK2A* vector (0.1 μg/mL) was mixed with Lipofectamine 2000 (Invitrogen) and then added to culture medium. Inhibitors were added 24 hours after the transfection. PCMV6-XL6 vector (OriGene) was used as a negative control. To determine the effect of Ca^{2+} on myofibroblast transformation, dcSSc dermal fibroblasts were cultured in Ca^{2+}-containing or Ca^{2+}-free DMEM. In a separate experiment, dcSSc fibroblasts cultured in Ca^{2+}-containing RPMI medium were treated with BAPTA-AM (20 μM; Thermo Fisher Scientific) in the presence or absence of 1 μM JQ1 for 2 days.

Western blots. Western blotting was performed following the protocol as described previously (39). Equal amounts of protein were separated by SDS-PAGE, then transferred to a nitrocellulose membrane. After blocking, the blots were probed with Abs against BRD2 (Abcam ab139690; clone EPR7642), BRD3 (Santa Cruz Biotechnology sc-81202; clone 2088C3a), BRD4 (Abcam ab128874; clone EPR5150[2]), collagen I (Abcam ab6308; clone COL-1), or α-SMA (Abcam ab5694). For loading control, the blots were immunoblotted with Abs against β-actin (MilliporeSigma A2066) or GAPDH (Cell Signaling Technology 2118; clone 14C10) as controls. Band quantification was performed using ImageJ (NIH) (40).

mRNA extraction and quantitative real-time PCR. Total RNA was extracted using Direct-zol RNA MiniPrep Kit (Zymo Research) before being converted to cDNA. Quantitative PCR was performed in a ViiA 7 Real-Time PCR System.

Cell proliferation assays. Proliferation of dermal fibroblasts was measured using the BrdU Cell Proliferation Assay Kit (BioVision). After 4 hours of BrdU incubation, cells were fixed before adding Abs and substrate. The absorbance at 450 nm was measured. In a separate experiment, the Incucyte live-cell imaging system (Sartorius) was used to monitor cell proliferation. Cells were seeded and allowed to grow overnight. After adding different treatments, cells were monitored by Incucyte up to 5 days. Cell counts were analyzed by the Incucyte S3 Analysis software (Sartorius).

Gel contraction and cell migration assays. The Cell Contraction Assay Kit (Cell Biolabs) was used for gel contraction (39). After treatment, cells were suspended and mixed with collagen solution. Solidified gels were lifted after 24 hours, and the areas of the gels were quantified using ImageJ (40). To evaluate the effect of JQ1 on cell migration, we performed a scratch-wound assay using the Incucyte live-cell imaging system. Cell migration was monitored by Incucyte up to 7 days.

Detection of apoptosis. To assess the effect of JQ1 on cell apoptosis, cells were plated in 96-well plates and treated with JQ1 in the presence of Incucyte Caspase 3/7 Apoptosis Reagent. The apoptotic cells were quantified by measuring cells with green fluorescence staining. The data were presented as the number of green fluorescing cells normalized to total cell count.

Cell cycle analysis. Fibroblasts were treated with 1 μM JQ1 for 48 hours, and the nontreated dcSSc fibroblasts were used as controls. Both the JQ1-treated and nontreated cells were first synchronized using the double thymidine block method before treatment (41). Cells were then harvested and stained with 7-aminoactinomycin D (7-AAD) viability dye and Vybrant DyeCycle Violet (both from Invitrogen) according to the manufacturer's protocol. The stained cells were analyzed using a BD FACSCanto II flow cytometer. Cell cycle analysis was performed on gated 7-AAD–live cells using FlowJo 7.0.

RNA-Seq and analysis. RNA-Seq was performed on mRNA extracted from control or JQ1-treated (1 μM) dcSSc fibroblasts. Samples with an RNA integrity number of more than 7 were subjected to library preparation and sequencing to 151 paired-end cycles on the NovaSeq 6000 platform (Illumina), resulting in approximately

35 million reads per sample. Differential gene expression analysis was performed using DESeq2 (42), using a negative binomial generalized linear model (thresholds: linear fold change greater than 1.5 or less than –1.5, Benjamini-Hochberg FDR-adjusted $P < 0.05$). Plots were generated using variations of DESeq2 plotting functions and other packages with R, version 3.3.3. Functional analysis, including candidate pathways activated or inhibited in comparison(s) and Gene Ontology (GO) term enrichments, was performed using iPathway Guide (Advaita) (43). Additional functional enrichment analyses to generate networks for visualization were performed using ClueGO (version 2.5.7)/CluePedia (version 1.5.7) (44, 45) and Cytoscape (v3.8.0) (46).

Intracellular Ca^{2+} measurement. Dermal fibroblasts from patients with dcSSc were treated with or without 1 μM JQ1, AZD5153, ARV825, or BIC1 for 48 hours before being collected for Ca^{2+} measurement by flow cytometry. Detached cells (1×10^7/mL) were labeled in loading buffer (HBSS with 1% FBS, 1 mM $CaCl_2$, and 1 mM $MgCl_2$) containing 1 μM Fluo-4 AM (Thermo Fisher Scientific) with 0.02% Pluronic F-127 at 37°C for 30 minutes with gentle agitation every 10 minutes. The labeled cells were washed twice with loading buffer containing 0.1 mM sulfinpyrazone (MilliporeSigma) and resuspended in the same loading buffer with sulfinpyrazone at 1×10^6/mL, incubated at 37°C for 30 minutes before basal fluorescence of Fluo-4 was measured on a BD FACSCanto II flow cytometer. Mean fluorescence intensity of unlabeled cells was subtracted from the mean fluorescence intensity of the labeled cells.

Data availability. All data relevant to the study are included in the article. The RNA-Seq data are deposited in the National Center for Biotechnology Information's Gene Expression Omnibus (GSE186961).

Statistics. A normality test was conducted to determine whether the data were normally distributed or skewed. To determine the differences between groups, unpaired 2-tailed *t* test, Mann-Whitney *U* test, paired 2-tailed *t* test, Wilcoxon's test, 1-way ANOVA with Holm-Šidák test, Kruskal-Wallis test with Dunn's test, or 2-way ANOVA with Dunnett's test were performed using GraphPad Prism, version 8 (GraphPad Software). $P < 0.05$ was considered statistically significant. Results were expressed as mean ± SD.

Study approval. This study was approved by the University of Michigan IRB. Written informed consent was received from participants prior to inclusion in the study. All animal protocols were approved for use from the University of Michigan IACUC.

Author contributions

All authors participated in the interpretation of study results and in the drafting, critical revision, and approval of the final version of the manuscript. PST, AHS, DAF, YMD, and DK contributed to study conception and/or design. SV, MGR, MNM, WDB, SM, PJP, MA, PLC, MAA, JHR, QW, ENM, DMR, JLH, and PT contributed to the acquisition of study results. SV, PJP, MA, QW, and PT contributed to the analysis of study results.

Acknowledgments

This work was supported by the funds from the American Autoimmune Related Disease Foundation and the Edward T. and Ellen K. Dryer Early Career Professorship (to PST); Chugai, PCORI, Novartis, Sanofi-Genzyme, and Genentech (to YMD); NIH/National Institute of Arthritis and Musculoskeletal and Skin Diseases (grant K24AR063120 to DK, grant T32AR007080 to MGR, and grant R01AR070148 to AHS); and NIH/National Institute of Allergy and Infectious Diseases (grants UM1-AI110557-05 and UM1-AI144298-01 to YMD and grant R01AI097134 to AHS).

Address correspondence to: Pei-Suen Tsou, Division of Rheumatology, University of Michigan, 109 Zina Pitcher Place, 4025 BSRB, Ann Arbor, Michigan 48109, USA. Phone: 734.647.1192; Email: ptsou@umich.edu.

1. Tsou PS. Epigenetic control of scleroderma: current knowledge and future perspectives. *Curr Rheumatol Rep*. 2019;21(12):69.
2. Tsou PS, et al. Inhibition of EZH2 prevents fibrosis and restores normal angiogenesis in scleroderma. *Proc Natl Acad Sci U S A*. 2019;116(9):3695–3702.
3. Bergmann C, et al. The histone demethylase Jumonji domain-containing protein 3 (JMJD3) regulates fibroblast activation in systemic sclerosis. *Ann Rheum Dis*. 2018;77(1):150–158.
4. Kramer M, et al. Inhibition of H3K27 histone trimethylation activates fibroblasts and induces fibrosis. *Ann Rheum Dis*. 2013;72(4):614–620.
5. Xiong C, et al. Pharmacological targeting of BET proteins inhibits renal fibroblast activation and alleviates renal fibrosis. *Oncotarget*. 2016;7(43):69291–69308.

6. Zhou B, et al. Brd4 inhibition attenuates unilateral ureteral obstruction-induced fibrosis by blocking TGF-β-mediated Nox4 expression. *Redox Biol*. 2017;11:390–402.
7. Ding N, et al. BRD4 is a novel therapeutic target for liver fibrosis. *Proc Natl Acad Sci U S A*. 2015;112(51):15713–15718.
8. Tang X, et al. BET bromodomain proteins mediate downstream signaling events following growth factor stimulation in human lung fibroblasts and are involved in bleomycin-induced pulmonary fibrosis. *Mol Pharmacol*. 2013;83(1):283–293.
9. Alqahtani A, et al. Bromodomain and extra-terminal motif inhibitors: a review of preclinical and clinical advances in cancer therapy. *Future Sci OA*. 2019;5(3):FSO372.
10. Feng J, et al. Ca $^{2+}$ signaling in cardiac fibroblasts and fibrosis-associated heart diseases. *J Cardiovasc Dev Dis*. 2019;6(4):34.
11. Skelding KA, et al. Controlling the cell cycle: the role of calcium/calmodulin-stimulated protein kinases I and II. *Cell Cycle*. 2011;10(4):631–639.
12. Delmore JE, et al. BET bromodomain inhibition as a therapeutic strategy to target c-Myc. *Cell*. 2011;146(6):904–917.
13. Shin JY, et al. Epigenetic activation and memory at a *TGFB2* enhancer in systemic sclerosis. *Sci Transl Med*. 2019;11(497):eaaw0790.
14. Klein K. Bromodomain protein inhibition: a novel therapeutic strategy in rheumatic diseases. *RMD Open*. 2018;4(2):e000744.
15. Morgado-Pascual JL, et al. Bromodomain and extraterminal proteins as novel epigenetic targets for renal diseases. *Front Pharmacol*. 2019;10:1315.
16. Mietton F, et al. Selective BET bromodomain inhibition as an antifungal therapeutic strategy. *Nat Commun*. 2017;8(1):15482.
17. Andrieu GP, et al. BET proteins in abnormal metabolism, inflammation, and the breast cancer microenvironment. *J Leukoc Biol*. 2018;104(2):265–274.
18. Donati B, et al. BRD4 and cancer: going beyond transcriptional regulation. *Mol Cancer*. 2018;17(1):164.
19. Kumar K, et al. BET inhibitors block pancreatic stellate cell collagen I production and attenuate fibrosis in vivo. *JCI Insight*. 2017;2(3):e88032.
20. Mukherjee S, et al. Disruption of calcium signaling in fibroblasts and attenuation of bleomycin-induced fibrosis by nifedipine. *Am J Respir Cell Mol Biol*. 2015;53(4):450–458.
21. Chung CC, et al. Calcium regulation on the atrial regional difference of collagen production activity in atrial fibrogenesis. *Biomedicines*. 2021;9(6):686.
22. Zhang W, et al. Inhibition of calcium-calmodulin-dependent kinase II suppresses cardiac fibroblast proliferation and extracellular matrix secretion. *J Cardiovasc Pharmacol*. 2010;55(1):96–105.
23. Wei C, et al. Calcium flickers steer cell migration. *Nature*. 2009;457(7231):901–905.
24. Tupper JT, et al. Membrane transport properties differ following return of serum-deprived versus Ca++-deprived human fibroblasts to a proliferative state. *J Cell Physiol*. 1982;110(1):29–34.
25. Chakraborty D, et al. Fibroblast growth factor receptor 3 activates a network of profibrotic signaling pathways to promote fibrosis in systemic sclerosis. *Sci Transl Med*. 2020;12(563):eaaz5506.
26. Tian X, et al. ANO1 regulates cardiac fibrosis via ATI-mediated MAPK pathway. *Cell Calcium*. 2020;92:102306.
27. Ding Z, et al. Ryanodine receptor type 2 plays a role in the development of cardiac fibrosis under mechanical stretch through TGFβ-1. *Int Heart J*. 2017;58(6):957–961.
28. Lin BL, et al. In vivo selective inhibition of TRPC6 by antagonist BI 749327 ameliorates fibrosis and dysfunction in cardiac and renal disease. *Proc Natl Acad Sci U S A*. 2019;116(20):10156–10161.
29. Adapala RK, et al. TRPV4 channels mediate cardiac fibroblast differentiation by integrating mechanical and soluble signals. *J Mol Cell Cardiol*. 2013;54:45–52.
30. Kreusser MM, et al. Inducible cardiomyocyte-specific deletion of CaM kinase II protects from pressure overload-induced heart failure. *Basic Res Cardiol*. 2016;111(6):65.
31. Zhong P, et al. Role of CaMKII in free fatty acid/hyperlipidemia-induced cardiac remodeling both in vitro and in vivo. *J Mol Cell Cardiol*. 2017;109:1–16.
32. Winters CJ, et al. CaMKII inhibition in type II pneumocytes protects from bleomycin-induced pulmonary fibrosis by preventing Ca2+-dependent apoptosis. *Am J Physiol Lung Cell Mol Physiol*. 2016;310(1):L86–L94.
33. Zeng MQ, et al. Verapamil inhibits ureteral scar formation by regulating CaMK II-mediated Smad pathway. *Chem Biol Interact*. 2021;346:109570.
34. Zhou J, et al. NMDA receptor-mediated CaMKII/ERK activation contributes to renal fibrosis. *BMC Nephrol*. 2020;21(1):392.
35. Lee DU, et al. Nonselective inhibition of the epigenetic transcriptional regulator BET induces marked lymphoid and hematopoietic toxicity in mice. *Toxicol Appl Pharmacol*. 2016;300:47–54.
36. Filippakopoulos P, et al. Selective inhibition of BET bromodomains. *Nature*. 2010;468(7327):1067–1073.
37. Kahl DJ, et al. 5-Aryl-1,3,4-oxadiazol-2-ylthioalkanoic acids: a highly potent new class of inhibitors of rho/myocardin-related transcription factor (MRTF)/serum response factor (SRF)-mediated gene transcription as potential antifibrotic agents for scleroderma. *J Med Chem*. 2019;62(9):4350–4369.
38. Van den Hoogen F, et al. 2013 classification criteria for systemic sclerosis: an American college of rheumatology/European league against rheumatism collaborative initiative. *Ann Rheum Dis*. 2013;72(11):1747–1755.
39. Tsou PS, et al. Identification of cysteine-rich angiogenic inducer 61 as a potential antifibrotic and proangiogenic mediator in scleroderma. *Arthritis Rheumatol*. 2019;71(8):1350–1359.
40. Schneider CA, et al. NIH image to ImageJ: 25 years of image analysis. *Nat Methods*. 2012;9(7):671–675.
41. Chen G, Deng X. Cell synchronization by double thymidine block. *Bio Protoc*. 2018;8(17):e2994.
42. Love MI, et al. Moderated estimation of fold change and dispersion for RNA-seq data with DESeq2. *Genome Biol*. 2014;15(12):550.
43. Draghici S, et al. A systems biology approach for pathway level analysis. *Genome Res*. 2007;17(10):1537–1545.
44. Bindea G, et al. ClueGO: a Cytoscape plug-in to decipher functionally grouped gene ontology and pathway annotation networks. *Bioinformatics*. 2009;25(8):1091–1093.
45. Bindea G, et al. CluePedia Cytoscape plugin: pathway insights using integrated experimental and in silico data. *Bioinformatics*. 2013;29(5):661–663.
46. Shannon P, et al. Cytoscape: a software environment for integrated models of biomolecular interaction networks. *Genome Res*. 2003;13(11):2498–2504.